Diffraction from deformed volume holograms: perturbation theory approach

Kehan Tian and Thomas Cuingnet

Department of Mechanical Engineering, Massachusetts Institute of Technology, 77 Massachusetts Avenue, Room 3-461c, Cambridge, Massachusetts 02139

Zhenyu Li

Department of Electrical Engineering, California Institute of Technology, Pasadena, California 91125

Wenhai Liu

Ondax, Inc., 850 East Duarte Road, Monrovia, California 91016

Demetri Psaltis

Department of Electrical Engineering, California Institute of Technology, Pasadena, California 91125

George Barbastathis

Department of Mechanical Engineering, Massachusetts Institute of Technology, 77 Massachusetts Avenue, Room 3-461c, Cambridge, Massachusetts 02139

Received March 7, 2005; accepted May 11, 2005

We derive the response of a volume grating to arbitrary small deformations, using a perturbative approach. This result is of interest for two applications: (a) when a deformation is undesirable and one seeks to minimize the diffracted field's sensitivity to it and (b) when the deformation itself is the quantity of interest and the diffracted field is used as a probe into the deformed volume where the hologram was originally recorded. We show that our result is consistent with previous derivations motivated by the phenomenon of shrinkage in photopolymer holographic materials. We also present the analysis of the grating's response to deformation due to a point indenter and present experimental results consistent with theory. © 2005 Optical Society of America

OCIS codes: 090.7330, 120.3940.

1. INTRODUCTION

Deformation of volume holograms, such as shrinkage during processing,[1,2] or elastic deformation due to the action of force can cause deviation in the angle or wavelength for the Bragg matching condition[3,4] and aberrations in the reconstructed image.[5] This problem, usually associated with the investigation of holographic materials, has received much attention since holography was invented.[6,7] It is a significant source of concern in application areas such as holographic memories,[8,9] information processing,[10] interconnects,[11] and imaging applications.[12] For example, researchers have investigated polymer materials with minimal shrinkage[13–16] and methods to compensate the deviation due to shrinkage.[17,18] Based on shrinkage only, the models used in the literature are relatively simple, treating linear deformation only. In this paper, we present a generalized theory that can deal with arbitrary deformations.

Deformation can be thought of as a two-sided problem: One side is how to avoid deformation, the other is how to measure it. Deformation measurement has been intensively investigated during the past 30 years,[19–23] but it has been exclusively limited to two-dimensional (2D) measurements of surface deformation. The universal principle applied to this problem consists of first producing an interferogram, i.e., modulating a signature of the surface before deformation as a phase modulation on an optical carrier. When the interferogram is mixed with the signature of the deformed surface, the beat term corresponds to the difference, i.e., the deformation. The mixing can be performed optically or digitally. Optical mixing is usually referred to as "holographic interferometry"[19,20] if the beating is with an interferogram recorded on photographic film and as moiré interferometry[22,23] if the beating is between two sets of intensity fringes recorded on a digital camera. Digital mixing is called "speckle interferometry,"[21] where the speckle is interpreted as a random phase mask; then the beating is the cross-correlation function of the mask before and after deformation. Digital holography[24,25] can also be thought of in similar terms, especially in the context of holographic particle image velocimetry,[26,27] where instead of deformation one measures displacement of particles in a thin sheet of moving fluid.

1084-7529/05/122880-10/$15.00

Three-dimensional (3D) deformation measurement is more challenging because the mixing and beating must occur throughout an entire volume as the optical fields propagate through. This eliminates both film and digital cameras as possible media for recording the interferograms. In this paper, we propose instead the use of Bragg diffraction for 3D deformation measurement. The mixing step is the recording of a volume hologram in a transparent 3D medium before it is deformed. The hologram is then reconstructed in the presence of an unknown 3D deformation, and the diffracted intensity is captured on a digital camera. Examples are shrinkage, shear, compression, indentation, crack propagation, etc. Assuming that the deformation is not severe enough to destroy the optical quality of the medium, the diffracted field is, in effect, the 3D beat between the deformed and undeformed versions.

Since the diffracted intensity is measured on a digital camera, which is a 2D medium, the beating signature is captured as a *projection* rather than a direct image. This implies that, in general, more than one measurement is required to capture the complete 3D deformation field. Nevertheless, our proposed technique is the first measurement method, to our knowledge, that is explicitly designed to handle 3D deformations in optically transparent media.

In this paper, we deal exclusively with the "forward" problem of establishing the beat field when the volume hologram and the 3D deformation are both known. Surprisingly, there have been no efforts to that end in the literature to date, except for the special case of linear shrinkage. Here we provide general expressions that are applicable to arbitrary deformations under a set of mildly restrictive assumptions, such as preservation of the average index of refraction and validity of the first-order Born approximation. The derivation is carried out in Section 2 for small deformations for which a perturbative approach is adequate, and in a more general (but also more algebraically complex) form in Appendixes A and B. In Section 3, we confirm that the general theory matches with the well-known predictions and observations of shrinkage effects from the literature. In Section 4, we carry out the modeling of the diffracted field and report experimental results in the case of a deformation produced by an indenter tip applied against the surface of a semi-infinite slab. The experiments match very well with the theory.

The solution to the forward problem, which we are presenting here, is always the first step before the "inverse" problem, i.e., the measurement of arbitrary deformations from a set of diffracted intensity measurements in our case, can be attacked. The inverse problem usually poses additional challenges involving the efficacy of the measurement and the well-posedness of the solution. This will very clearly be the case in our approach, since the measurement is that of a projection, as we already noted. Fortunately, in many cases of interest, including the indentation problem, existing analytical or numerical models of 3D deformation can be used to extract deformation parameters even from a single measurement. In these cases, the formulation presented in this paper is adequate.

2. PERTURBATION THEORY ON THE DEFORMATION OF VOLUME HOLOGRAMS

Consider a volume hologram with dielectric modulation $\Delta\epsilon(x,y,z)$ that changes to $\Delta\epsilon'(x',y',z')$ after deformation, as shown in Fig. 1. Our goal is to derive an expression for the diffracted field when the deformed hologram is probed by an arbitrary light field. With the assumption that the dielectric constant of each point inside the hologram does not change when that point moves due to the deformation, we can express $\Delta\epsilon'(x',y',z')$ as

$$\Delta\epsilon'(x',y',z') = \Delta\epsilon(f_x(x',y',z'),f_y(x',y',z'),f_z(x',y',z')), \tag{1}$$

where $\mathbf{f}(\mathbf{r}') = \hat{\mathbf{x}}f_x(x',y',z') + \hat{\mathbf{y}}f_y(x',y',z') + \hat{\mathbf{z}}f_z(x',y',z')$ is the former position of the point at $\mathbf{r}' = \hat{\mathbf{x}}x' + \hat{\mathbf{y}}y' + \hat{\mathbf{z}}z'$, and it can be obtained from the strain or displacement functions. This assumption is valid when the deformation is not large enough to affect the material properties of the hologram. We refer to these weak deformations as "conformal." The conformality condition is satisfied for most cases. An expression for the diffracted field for general nonconformal deformations is given in Appendix A.

Returning to the case of conformal deformation, we write Eq. (1) in vector form as

$$\Delta\epsilon'(\mathbf{r}') = \Delta\epsilon(\mathbf{f}(\mathbf{r}')). \tag{2}$$

When the displacement is analytic, we can approximate Eq. (2) by Nth-order Taylor expansion as

$$\Delta\epsilon(\mathbf{f}(\mathbf{r}')) \approx \Delta\epsilon(\mathbf{r}') + \sum_{j=1}^{N} \frac{\{[\mathbf{f}(\mathbf{r}') - \mathbf{r}'] \cdot \nabla\}^j}{j!} \Delta\epsilon(\mathbf{r}'). \tag{3}$$

Without loss of generality, we can restrict $\Delta\epsilon(\mathbf{r}')$ to a set of planar, parallel grating fringes recorded by two intersecting plane waves: reference beam $E_f(\mathbf{r}) = \exp(i\mathbf{k}_f \cdot \mathbf{r})$ and signal beam $E_S(\mathbf{r}) = \exp(i\mathbf{k}_S \cdot \mathbf{r})$. This is because any hologram can be regarded as a linear superposition of infinite plane-wave holograms.[28] In most cases, the superposition is straightforward and numerically stable. We prefer the development of the perturbation theory using the plane-wave holograms because it leads to simpler, more intuitive expressions. The perturbation theory for non-plane-wave holograms is discussed in Appendix B. For a plane-wave hologram, the undeformed dielectric modulation can be written in analytic form as

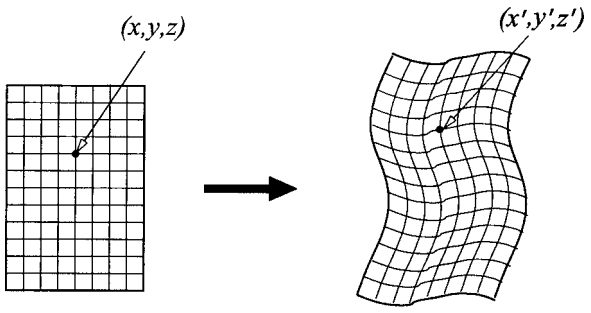

Fig. 1. Deformation of holograms.

$$\Delta\epsilon(\mathbf{r}') = \epsilon_1 \exp(i\mathbf{K}_g \cdot \mathbf{r}'), \tag{4}$$

where ϵ_1 is the amplitude of the spatial modulation expressing the hologram strength and $\mathbf{K}_g = \mathbf{k}_s - \mathbf{k}_f$ is the wave vector of the grating. Its jth-order derivative can be obtained as

$$\nabla^j \Delta\epsilon(\mathbf{r}') = (i\mathbf{K}_g)^j \Delta\epsilon(\mathbf{r}'), \tag{5}$$

$$\nabla \to i\mathbf{K}_g. \tag{6}$$

Substituting expression (6) into relation (3), we obtain

$$\Delta\epsilon(\mathbf{f}(\mathbf{r}')) \approx \Delta\epsilon(\mathbf{r}') + \sum_{j=1}^{N} \frac{[\Delta\mathbf{f}(\mathbf{r}') \cdot i\mathbf{K}_g]^j}{j!} \Delta\epsilon(\mathbf{r}'), \tag{7}$$

where $\Delta\mathbf{f}(\mathbf{r}') = \mathbf{f}(\mathbf{r}') - \mathbf{r}'$ is the displacement due to the deformation. The displacement can be expressed as

$$\Delta\mathbf{f}(\mathbf{r}') = \begin{pmatrix} \Delta f_x(x',y',z') \\ \Delta f_y(x',y',z') \\ \Delta f_z(x',y',z') \end{pmatrix} = \begin{bmatrix} a_{11} & a_{12} & a_{13} \\ a_{21} & a_{22} & a_{23} \\ a_{31} & a_{32} & a_{33} \end{bmatrix} \begin{pmatrix} x' \\ y' \\ z' \end{pmatrix} = A \cdot \mathbf{r}', \tag{8}$$

where, in general, a_{kl} is a function of (x',y',z') for all k, $l = 1,2,3$. The matrix A is referred to as the "strain matrix" or "deformation matrix." In special cases, e.g., uniform shrinkage of a volume hologram, A is constant and very simple expressions for the diffracted field can be derived. Our analysis remains valid for constant as well as nonconstant deformation matrices. Using Eq. (8), we can write relation (7) as

$$\Delta\epsilon(\mathbf{f}(\mathbf{r}')) \approx \Delta\epsilon(\mathbf{r}') + \sum_{j=1}^{N} \frac{(\mathbf{K}_g \cdot A \cdot i\mathbf{r}')^j}{j!} \Delta\epsilon(\mathbf{r}'). \tag{9}$$

Using Eq. (4), we can see that the dielectric modulation is a function not only of $\mathbf{r}'$ but also of $\mathbf{K}_g$. Therefore we can swap derivatives and write the conjugate of Eq. (5) and expression (6) as

$$\nabla_{\mathbf{K}_g}^j \Delta\epsilon(\mathbf{r}') = (i\mathbf{r}')^j \Delta\epsilon(\mathbf{r}'), \tag{10}$$

$$i\mathbf{r}' \to \nabla_{\mathbf{K}_g}. \tag{11}$$

By substituting expression (11) into relation (9), we can obtain the deformed dielectric modulation as

$$\Delta\epsilon(\mathbf{f}(\mathbf{r}')) \approx \Delta\epsilon(\mathbf{r}') + \sum_{j=1}^{N} \frac{(\mathbf{K}_g \cdot A \cdot \nabla_{\mathbf{K}_g})^j}{j!} \Delta\epsilon(\mathbf{r}'). \tag{12}$$

With the knowledge of the deformed dielectric modulation, we can calculate the diffracted field change in the Fourier geometry, as shown in Fig. 2. Before deformation, when an arbitrary probe beam $E_p(\mathbf{r})$ is used to read out the volume hologram, the diffracted field incident on the detector is[29]

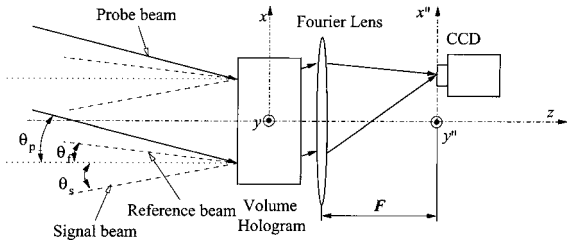

Fig. 2. Fourier geometry with plane-wave reference and plane-wave signal.

$$E_d(\mathbf{r}'') = \int\int\int E_p(\mathbf{r})\Delta\epsilon(\mathbf{r})V(\mathbf{r})\exp\left(-i\frac{2\pi}{\lambda}\frac{xx''+yy''}{F}\right) \times \exp\left[-i\frac{2\pi}{\lambda}\left(1-\frac{x''^2+y''^2}{2F^2}\right)z\right]d^3\mathbf{r}, \tag{13}$$

where the index function $V(\mathbf{r})$ is defined as

$$V(\mathbf{r}) = \begin{cases} 1 & \text{inside volume hologram} \\ 0 & \text{outside volume hologram} \end{cases}, \tag{14}$$

F is the focal length of the Fourier lens between the hologram and the detector, and $\mathbf{r}'' = \hat{\mathbf{x}}x'' + \hat{\mathbf{y}}y''$ is the coordinate on the camera plane. In fact, Eq. (13) is the 3D Fourier transform of $E_p(\mathbf{r})\Delta\epsilon(\mathbf{r})V(\mathbf{r})$ computed at spatial frequency coordinates $f_x = x''/(\lambda F), f_y = y''/(\lambda F), f_z = (1/\lambda)[1 - (x''^2+y''^2)/(2F^2)]$.

After deformation the diffracted field changes to

$$\tilde{E}_d(\mathbf{r}'') = \int\int\int E_p(\mathbf{r}')\Delta\epsilon'(\mathbf{r}')\tilde{V}(\mathbf{r}')\exp\left(-i\frac{2\pi}{\lambda}\frac{x'x''+y'y''}{F}\right) \times \exp\left[-i\frac{2\pi}{\lambda}\left(1-\frac{x''^2+y''^2}{2F^2}\right)z'\right]d^3\mathbf{r}'. \tag{15}$$

Since the hologram shape should remain approximately constant, except under very severe deformation, and in any case changes in index function affect only the boundary of the volume integral, we use the approximation $\tilde{V}(\mathbf{r}') \approx V(\mathbf{r})$. Thus by substituting Eq. (2) and relation (12) into Eq. (15), we can obtain

$$\tilde{E}_d(\mathbf{r}'') \approx E_d(\mathbf{r}'') + \int\int\int E_p(\mathbf{r}')\sum_{j=1}^{N}\frac{(\mathbf{K}_g \cdot A \cdot \nabla_{\mathbf{K}_g})^j}{j!}\Delta\epsilon(\mathbf{r}') \times V(\mathbf{r}')\exp\left(-i\frac{2\pi}{\lambda}\frac{x'x''+y'y''}{F}\right) \times \exp\left[-i\frac{2\pi}{\lambda}\left(1-\frac{x''^2+y''^2}{2F^2}\right)z'\right]d^3\mathbf{r}'. \tag{16}$$

Inside the integral, $\mathbf{K}_g$ and $\nabla_{\mathbf{K}_g}$ do not depend on $\mathbf{r}'$. Therefore, if the displacement can be linearized (A is a constant matrix), we can take $(\mathbf{K}_g \cdot A \cdot \nabla_{\mathbf{K}_g})^j/(j!)$ out of the integral and obtain the final result in a very simple form as

$$\tilde{E}_{\mathrm{d}}(\mathbf{r}'') \approx E_{\mathrm{d}}(\mathbf{r}'') + \sum_{j=1}^{N} \frac{(\mathbf{K}_{\mathrm{g}} \cdot A \cdot \nabla_{\mathbf{K}_{\mathrm{g}}})^{j}}{j!} E_{\mathrm{d}}(\mathbf{r}''). \tag{17}$$

In particular, for the first-order approximation in the Taylor series,

$$\tilde{E}_{\mathrm{d}}(\mathbf{r}'') \approx E_{\mathrm{d}}(\mathbf{r}'') + \mathbf{K}_{\mathrm{g}} \cdot A \cdot \nabla_{\mathbf{K}_{\mathrm{g}}} E_{\mathrm{d}}(\mathbf{r}''), \tag{18}$$

which is very similar to the standard form of the perturbation theory on electromagnetism.[30]

With relation (16) or (17), we can already perform the calculation of diffracted field change due to deformation. Before doing so, it is worthwhile to look at these equations qualitatively in some detail. The first interesting result is that $\mathbf{K}_{\mathrm{g}} \cdot A \cdot \nabla_{\mathbf{K}_{\mathrm{g}}}$ has null space when $A^{\mathrm{T}} \cdot \mathbf{K}_{\mathrm{g}}$ is perpendicular to $\nabla_{\mathbf{K}_{\mathrm{g}}}$ or $A^{\mathrm{T}} \cdot \mathbf{K}_{\mathrm{g}}$ is equal to zero, meaning that there exist holograms that have zero response for a given deformation. For example, if there is a hologram with its grating fringes along the z direction (the wave vector of the grating $\mathbf{K}_{\mathrm{g}}$ is in the x–y plane), the deformation along the z direction will have no effect on it. This is intuitively obvious, and it is useful if we desire to minimize the effect of an anticipated deformation (e.g., shrinkage) on the hologram. Second, if our goal is to measure a certain deformation, then we can find some optimal holograms that have maximum sensitivity to that deformation. The condition is

$$(A^{\mathrm{T}} \cdot \mathbf{K}_{\mathrm{g}}) \parallel \nabla_{\mathbf{K}_{\mathrm{g}}}. \tag{19}$$

Condition (19) also has an intuitive interpretation with the help of a K-sphere, as shown in Fig. 3. Usually when the probe beam is Bragg matched before deformation, i.e., $E_{\mathrm{p}}(\mathbf{r}) = \exp(i\mathbf{k}_{\mathrm{f}} \cdot \mathbf{r})$, the strongest dependence of E_{d} on $\mathbf{K}_{\mathrm{g}}$ occurs when a change in $\mathbf{K}_{\mathrm{g}}$ leads to Bragg mismatch fastest. The mismatch $\Delta\mathbf{K}_{\mathrm{g}}$ is fastest when the tip of the grating vector after deformation moves as fast as possible away from the K-sphere, which is along the direction connecting the center of the K-sphere to the tip of the grating vector on the K-sphere. This is actually the same as the direction of the signal beam $\mathbf{k}_{\mathrm{S}}$. The locus of the maximum Bragg mismatch as a function of different deformations δ is calculated in Appendix C, where it is shown that the maximum Bragg mismatch direction angle θ_δ is

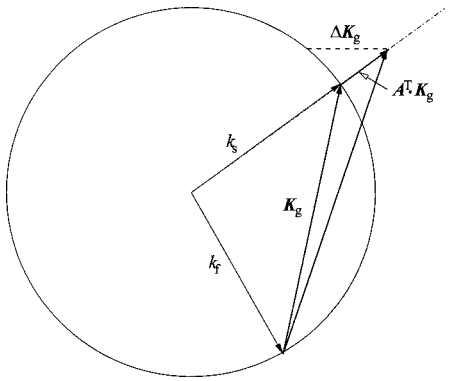

Fig. 3. K-sphere explanation of condition (19).

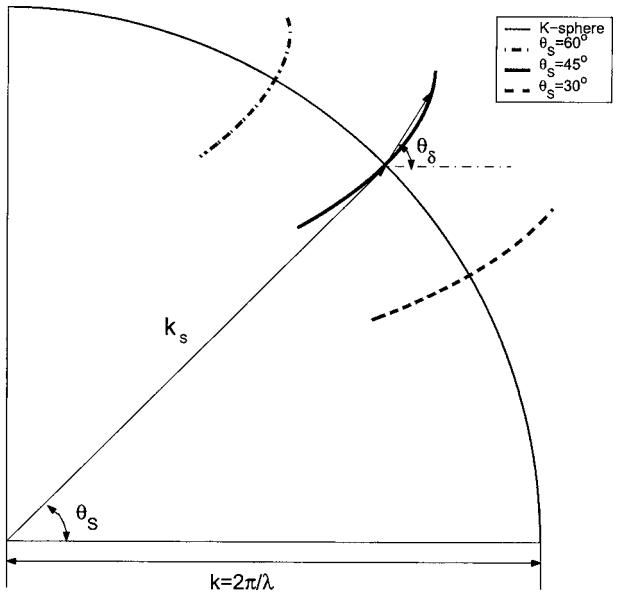

Fig. 4. Locus of maximum Bragg mismatch.

$$\sin\theta_\delta = \frac{k \sin\theta_{\mathrm{S}}}{k - \delta}, \tag{20}$$

where $k = 2\pi/\lambda$ is the wave number and θ_{S} is the direction angle of the signal beam. The sketch of the locus of the maximum Bragg mismatch is shown in Fig. 4.

From another point of view, $\nabla_{\mathbf{K}_{\mathrm{g}}} E_{\mathrm{d}}(\mathbf{r}'')$ means the gradient of $E_{\mathrm{d}}(\mathbf{r}'')$ on $\mathbf{K}_{\mathrm{g}}$. If the plane-wave hologram with grating vector $\mathbf{K}_{\mathrm{g}}$ is probed by $E_{\mathrm{p}}(\mathbf{r}) = \exp(i\mathbf{k}_{\mathrm{p}} \cdot \mathbf{r})$, then, without deformation, the diffracted field just after the hologram before the Fourier lens is[29]

$$\begin{aligned} E_{\mathrm{d}}(\mathbf{r}'') = \mathrm{sinc}\Bigg\{ & \frac{L}{2\pi}\Big[K_{\mathrm{g}z} + k_{\mathrm{p}z} \\ & - \sqrt{k^2 - (K_{\mathrm{g}x} + k_{\mathrm{p}x})^2 - (K_{\mathrm{g}y} + k_{\mathrm{p}y})^2}\Big] \Bigg\} \\ & \times \exp\{i[(K_{\mathrm{g}x} + k_{\mathrm{p}x})x'' + (K_{\mathrm{g}y} + k_{\mathrm{p}y})y'' \\ & + \sqrt{k^2 - (K_{\mathrm{g}x} + k_{\mathrm{p}x})^2 - (K_{\mathrm{g}y} + k_{\mathrm{p}y})^2} z'']\}, \end{aligned} \tag{21}$$

which is a plane wave with amplitude modulated by Bragg mismatch. Here, we assumed that the dimensions of the hologram are infinite in the x and y directions, and the thickness of the hologram is L. We can calculate the diffracted field gradient as

$$\begin{aligned} \nabla_{\mathbf{K}_{\mathrm{g}}} E_{\mathrm{d}}(\mathbf{r}'') \propto & (K_{\mathrm{g}x} + k_{\mathrm{p}x})\hat{x} + (K_{\mathrm{g}y} + k_{\mathrm{p}y})\hat{y} \\ & + \sqrt{k^2 - (K_{\mathrm{g}x} + k_{\mathrm{p}x})^2 - (K_{\mathrm{g}y} + k_{\mathrm{p}y})^2}\,\hat{z}, \end{aligned} \tag{22}$$

which is also along the direction connecting the center of the K-sphere to the tip of the grating vector, consistent with our earlier K-sphere analysis. According to condition (19), the deformed grating vector $A^{\mathrm{T}} \cdot \mathbf{K}_{\mathrm{g}}$ must point in this direction to achieve maximum change. Or if we want to measure a certain deformation A, the hologram whose grating vector $\mathbf{K}_{\mathrm{g}}$ satisfies condition (19) will have maximum sensitivity to this deformation A.

3. APPLICATION TO LINEAR DEFORMATION

Relations (17) and (18) can be applied to linear deformation directly, e.g., the shrinkage of holograms or compression by uniform pressure on the surface of holograms. The diffracted field after deformation can be calculated without a complicated and time-consuming integration.

The shrinkage of holograms has been observed to cause angular deviation and/or wavelength shift for maximum diffraction-efficiency reconstruction[3,4,17] and to cause aberrations.[5] With the perturbation theory discussed in Section 2, it can be investigated very conveniently.

Here, it is assumed that the shrinkage occurs only along the direction of the normal to the hologram's surface. A hologram of original thickness L shrinks to thickness L' such that

$$L' = (1-s)L, \tag{23}$$

where s is the coefficient of shrinkage. Thus, the displacement matrix is

$$A = \begin{bmatrix} 0 & 0 & 0 \\ 0 & 0 & 0 \\ 0 & 0 & s \end{bmatrix}. \tag{24}$$

If the plane-wave hologram with grating vector $\mathbf{K}_g$ is probed by $E_p(\mathbf{r}) = \exp(i\mathbf{k}_p \cdot \mathbf{r})$, then, without shrinkage, the diffracted field just after the hologram is given by Eq. (21). By substituting Eqs. (21) and (24) into perturbation formula (17), we can simplify the result after shrinkage to

$$\begin{aligned} \tilde{E}_d(\mathbf{r}'') &\approx E_d(\mathbf{r}'') + \sum_{j=1}^{N} \frac{\left(K_{gz} s \frac{\partial}{\partial K_{gz}}\right)^j}{j!} E_d(\mathbf{r}'') \\ &= \operatorname{sinc}\left\{ \frac{L}{2\pi}[(1+s)K_{gz} + k_{gz} \right. \\ &\quad \left. - \sqrt{k^2 - (K_{gx}+k_{px})^2 - (K_{gy}+k_{py})^2}] \right\} \\ &\quad \times \exp\{i[(K_{gx}+k_{px})x'' + (K_{gy}+k_{py})y'' \\ &\quad + \sqrt{k^2 - (K_{gx}+k_{px})^2 - (K_{gy}+k_{py})^2} z'']\}, \end{aligned} \tag{25}$$

which means that the shrinkage along the z direction affects only the efficiency and not the direction of the diffracted plane wave. This is consistent with the discussions in Refs. 3 and 17. Beyond this simple calculation, relation (17) can be used to predict the response of holograms deformed under any kind of affine transformations, including rotations, anisotropic shrinkage, etc.

4. APPLICATION TO NONLINEAR DEFORMATION

For holograms that undergo nonlinear deformation, we have to use the full 3D integral or Fourier transform in relation (16) to predict the diffracted field. To verify the validity of the perturbation theory on nonlinear deformation, we simulated the change in the diffracted field due to a point load exerted normally on the surface of a hologram. We also carried out an experiment and compared the results with the simulation.

When a concentrated point force P is acting normally to the surface of an elastic solid, as shown in Fig. 5(a), the elastic displacements at any point in the half-space are given by [31]

$$\begin{aligned} u_x &= \frac{P}{4\pi G}\left[\frac{xz}{\rho^3} - (1-2\nu)\frac{x}{\rho(\rho+z)}\right], \\ u_y &= \frac{P}{4\pi G}\left[\frac{yz}{\rho^3} - (1-2\nu)\frac{y}{\rho(\rho+z)}\right], \\ u_z &= \frac{P}{4\pi G}\left[\frac{z^2}{\rho^3} + \frac{2(1-\nu)}{\rho}\right], \end{aligned} \tag{26}$$

where G and ν are the shear modulus and Poisson ratio, respectively, and $\rho = \sqrt{x^2+y^2+z^2}$ is the distance of the point to the origin (loading position). The resulting deformation is shown in Fig. 5(b). The singularity at $\rho = 0$ is due to the δ-function nature of the point load. We can obtain the displacement matrix for each point in the deformed solid. Note that the displacement matrix elements are now position dependent, unlike the example in Section 3.

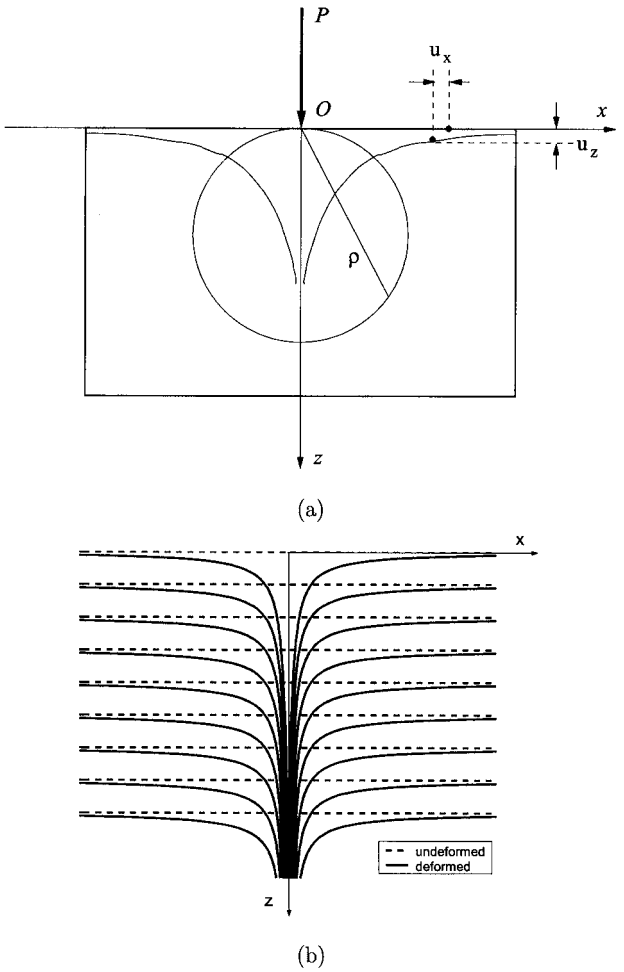

Fig. 5. Illumination of the deformation when a point load is exerted on the half-space.

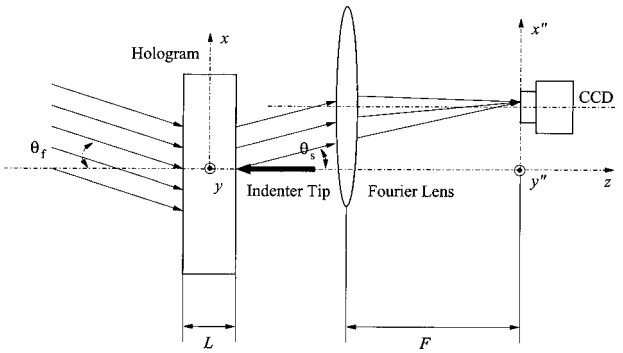

Fig. 6. Experiment geometry when a point load is exerted on a transmission hologram.

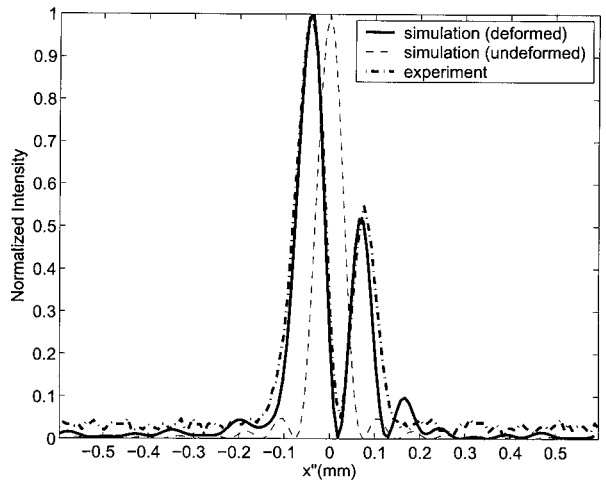

Fig. 7. Simulated and experimental results when a point load is exerted on a transmission hologram. Parameters are the wavelength $\lambda=488$ nm, the angle of reference beam $\theta_f=-7.5°$, the angle of signal beam $\theta_S=20°$, the thickness of the hologram $L=2$ mm, the estimated force $P=700$ N, and the focal length of the Fourier lens $F=400$ mm. The intensities before and after deformation were each normalized by their own maximum. The maximum intensity after deformation is 19.65% of the maximum intensity before deformation.

We constructed an experimental setup to verify the validity of the approach presented above. The holographic material was provided by Ondax, Inc. It had thickness $L=2$ mm and measured shear modulus $G=44$ GPa, with Poisson ratio $\nu=0.22$. The hologram was of the transmission type with reference and signal beam angles $\theta_f=-7.5°$ and $\theta_S=20°$, respectively, at a wavelength of 488 nm. The geometry of the experiment is shown in Fig. 6 with $F=400$ mm. The hologram was illuminated at the Bragg matching angle. A PULNiX TM-7EX CCD with 768×494 pixels (pixel size 8.4 μm$\times$9.8 μm) was used to observe the diffracted intensity. The hologram was deformed by using a diamond indenter tip applied normally against the back surface of the hologram. The deformation due to an indenter tip is in good agreement with the point load described by Eqs. (26), except near the singularity point $\rho=0$. Our experimental approach did not require force measurement; we estimated the force by using the displacement reading in the indenter carrier. During the experiment, we used the same probe beam, which is Bragg matched before deformation, to illuminate the hologram.

First, we simulated the expected change in diffracted field according to relation (16) and Eqs. (26). The results are shown in Fig. 7. An interesting observation is that the diffracted spot splits into twin peaks due to the point-load deformation. This can be explained intuitively based on the deformed fringe patterns of Fig. 8 and the K-sphere of Fig. 9 as follows. From Fig. 8, we see that the deformed grating is composed of two quasi-periodic fringe patterns symmetric with respect to the original grating fringes. The fringes are also curved, which is an indication of spatial chirp. If for the moment we neglect the spatial chirp, we obtain two gratings that are tilted with respect to the original grating, and also have smaller period because of the pressure applied by the indenter. Accordingly, we represent the twin gratings with wave vectors $\mathbf{K}_g'$ and $\mathbf{K}_g''$ that are tilted and elongated with respect to the original wave vector $\mathbf{K}_g$. Since we are reading out the hologram with the original reference $\mathbf{k}_f$, the twin peaks are expected to be Bragg mismatched. However, for small deformation, i.e., small deviations of the twin grating vector tips $\mathbf{K}_g'$ and $\mathbf{K}_g''$ from the K-sphere, we can still obtain diffraction from the partially mismatched gratings. The directions of the twin diffracted beams are denoted as $\mathbf{k}_d'$

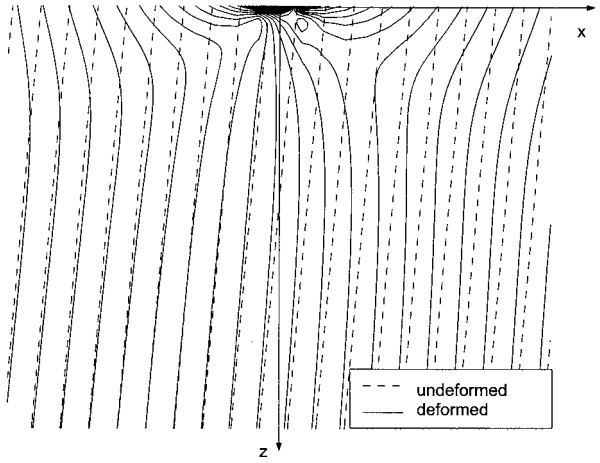

Fig. 8. Fringe patterns of a transmission hologram due to point load; the parameters are the same as those for Fig. 7.

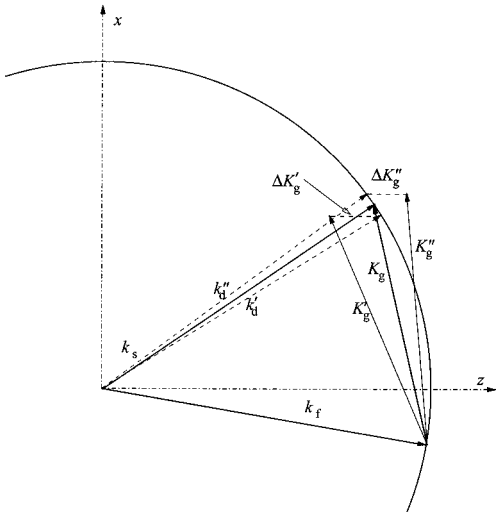

Fig. 9. K-sphere explanation for the twin peaks.

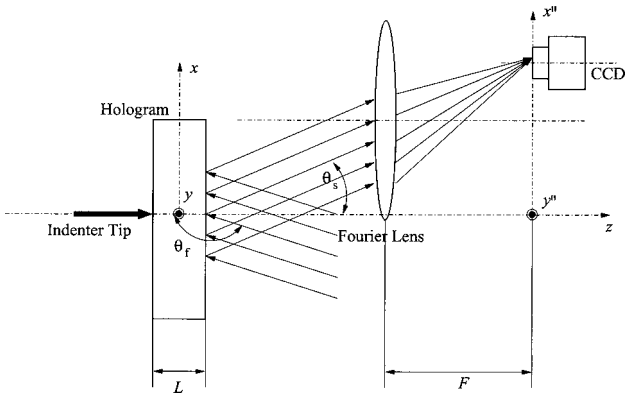

Fig. 10. Experiment geometry when a point load is exerted on a reflection hologram.

and $\mathbf{k}_d''$ in Fig. 9; they give rise to our observed twin peak on the CCD camera after Fourier transformation by the lens. Because the Bragg mismatch amounts $\Delta\mathbf{K}_g'$ and $\Delta\mathbf{K}_g''$ for the twin gratings are in general different, the twin diffracted beams have different efficiencies. The elevated sidelobes observed in Fig. 7 are due to the spatial chirp, which was neglected from the approximate explanation based on Fig. 9.

We performed our experiments by using an indenter tip moved by a micrometer to exert the point load on the hologram. The load position was exactly at the center of the aperture (the illumination area on the hologram). The experimental result obtained on the CCD camera is shown as the dotted–dashed curve in Fig. 7 and seen to be in agreement with the simulation. At the same time, we also observed some minor apodization effects mixed in with our experimental result: The sidelobes were suppressed, and the main lobes were a little wider. Because the apodization effect of volume holograms has been accounted for inherently in the perturbation theory, the additional apodization could be due to nonuniformity of holograms and probe beams.

We also performed simulations and experiments on a reflection-type hologram. The experimental geometry is shown in Fig. 10. The holographic material was also from Ondax, Inc., with the same shear modulus and Poisson ratio as those for the transmission hologram. The thickness of the reflection-type hologram was $L=1.5$ mm. The angles of reference beam and signal beam were $\theta_f=172°$ and $\theta_S=8°$, respectively, at a wavelength of 632 nm. The focal length of the Fourier lens was $F=400$ mm, and the hologram was also illuminated at the Bragg matching angle. The simulated and experimental results are shown in Fig. 11 and match very well. In this case, the diffracted field presents an almost symmetric pattern due to the point-load deformation. This can also be explained intuitively by the deformed fringe patterns of Fig. 12 and the *K*-sphere of Fig. 13 as follows. In this case, the original grating vector $\mathbf{K}_g$ is split into three gratings $\mathbf{K}_{g1}$, $\mathbf{K}_g'$, and $\mathbf{K}_g''$ after deformation. $\mathbf{K}_{g1}$ remains parallel to $\mathbf{K}_g$ but is longer because of the applied pressure. The two others, $\mathbf{K}_g'$ and $\mathbf{K}_g''$, are tilted and elongated as in the transmission case and have almost the same Bragg mismatch amounts $\Delta\mathbf{K}_g'$ and $\Delta\mathbf{K}_g''$. The result is a triplet peak, with a main lobe corresponding to the partially mismatched $\mathbf{K}_{g1}$ and two sidelobes corresponding to the partially mismatched $\mathbf{K}_g'$ and $\mathbf{K}_g''$. The sidelobes are weaker than the main lobe, while the amount of Bragg mismatch for $\mathbf{K}_g'$ and $\mathbf{K}_g''$ is larger than it is for $\mathbf{K}_{g1}$. In Fig. 11, we can also observe minor apodization effects mixed in with the experiment result, which is due to the same reasons as those in the transmission geometry.

It needs to be mentioned here that the repeatability of this experiment is not so good because of the difficulty in achieving the exact deformation of ideal point loading. First, we need to adjust the point load exactly at the center of the aperture. Second, the force must be normally exerted on the surface of the hologram. Third, we need enough stiffness of the whole supporting and holding systems. The deformation is very sensitive to these factors. So to get the deformation as close to the ideal as possible, the adjustment in the experiments must be very precise.

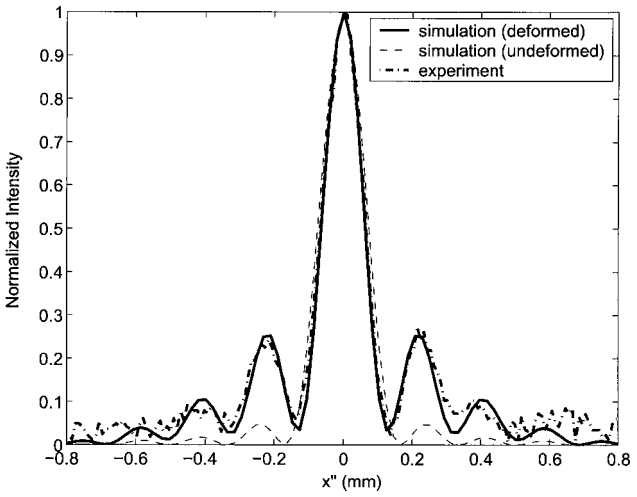

Fig. 11. Simulated and experimental results when a point load is exerted on a reflection hologram. Parameters are the wavelength $\lambda=632$ nm, the angle of reference beam $\theta_f=172°$, the angle of signal beam $\theta_S=8°$, the thickness of the hologram $L=1.5$ mm, the estimated force $P=19$ N, and the focal length of the Fourier lens $F=400$ mm. The intensities before and after deformation were each normalized by their own maximum. The maximum intensity after deformation is 34.55% of the maximum intensity before deformation.

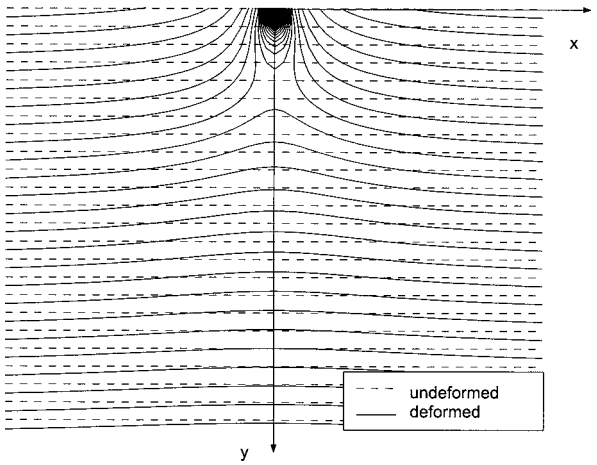

Fig. 12. Fringe patterns of a reflection hologram due to point load; the parameters are the same as those for Fig. 11.

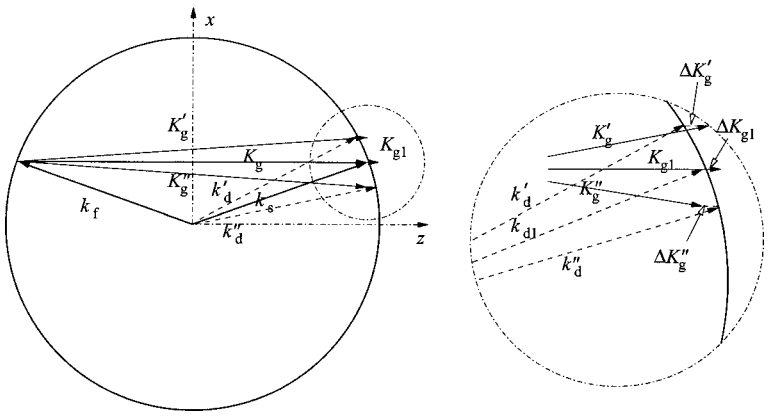

Fig. 13. *K*-sphere explanation for the "triplet peak."

5. CONCLUSIONS

We have derived a general solution to the problem of diffraction from a volume hologram that has been arbitrarily deformed compared with its recorded shape. We have shown that in many cases of interest, including shrinkage and indentation due to application of a point tip, a perturbation approach can predict accurately the diffracted field and can be used to establish deformation parameters by matching the experimental measurements with analytical or numerical models. Our approach is unique in that it projects the deformation from the entire 3D volume onto the measurement, and thus it has potential for measuring even more arbitrary deformations for which analytical or numerical predictions do not exist.

Our analysis in this paper is cast as a "forward problem," where the deformation is given and we seek the diffracted field. The future work will be the "inverse problem," which is to determine the deformation itself based on a set of observations of the field diffracted from a known (predeformation) volume hologram. Our *ab initio* model and perturbation theory make it possible to calculate the complicated patterns analytically or numerically for which the inverse problem will have high utility.

APPENDIX A: PERTURBATION THEORY CONSIDERING DIELECTRIC CONSTANT CHANGE DURING DEFORMATION

The conformality assumption that the dielectric constant does not change during deformation is valid when the deformation is not large enough to change the material properties of holograms. Although in some conditions the dielectric constant may change, we still can include this effect in our theory by modifying Eq. (2) as

$$\Delta\epsilon'(\mathbf{r}') = a(\mathbf{r}')\Delta\epsilon(\mathbf{f}(\mathbf{r}')), \tag{A1}$$

where $a(\mathbf{r}')$ is the amplitude change of dielectric modulation. Following the same derivation steps, we can easily find the diffracted field, considering the dielectric constant change during deformation as

$$\begin{aligned}\tilde{E}_d(\mathbf{r}'') \approx{}& \hat{E}_d(\mathbf{r}'') \\ &+ \int\int\int E_p(\mathbf{r}')a(\mathbf{r}')\sum_{j=1}^{N}\frac{(\mathbf{K}_g\cdot A\cdot\nabla_{\mathbf{K}_g})^j}{j!}\Delta\epsilon(\mathbf{r}') \\ &\times V(\mathbf{r}')\exp\left(-i\frac{2\pi}{\lambda}\frac{x'x''+y'y''}{F}\right) \\ &\times\exp\left[-i\frac{2\pi}{\lambda}\left(1-\frac{x''^2+y''^2}{2F^2}\right)z'\right]\mathrm{d}^3\mathbf{r}',\end{aligned} \tag{A2}$$

where

$$\begin{aligned}\hat{E}_d(\mathbf{r}'') = {}& \int\int\int E_p(\mathbf{r}')a(\mathbf{r}')\Delta\epsilon(\mathbf{r}')V(\mathbf{r}') \\ &\times\exp\left(-i\frac{2\pi}{\lambda}\frac{x'x''+y'y''}{F}\right) \\ &\times\exp\left[-i\frac{2\pi}{\lambda}\left(1-\frac{x''^2+y''^2}{2F^2}\right)z'\right]\mathrm{d}^3\mathbf{r}',\end{aligned} \tag{A3}$$

If the displacement is linear, then

$$\tilde{E}_d(\mathbf{r}'') \approx \hat{E}_d(\mathbf{r}'') + \sum_{j=1}^{N}\frac{(\mathbf{K}_g\cdot A\cdot\nabla_{\mathbf{K}_g})^j}{j!}\hat{E}_d(\mathbf{r}''). \tag{A4}$$

APPENDIX B: GENERALIZED PERTURBATION THEORY FOR ARBITRARY HOLOGRAMS

We can generalize relations (16) and (17) for arbitrary holograms that can be written as a linear superposition of many plane-wave holograms:

$$\begin{aligned}\Delta\epsilon(\mathbf{r}) &= \sum_{m,n,l}\epsilon_{mnl}\exp\left[i2\pi\left(\frac{mx}{L_x}+\frac{ny}{L_y}+\frac{lz}{L_z}\right)\right] \\ &= \sum_{m,n,l}\epsilon_{mnl}\exp[i\mathbf{K}_g^{(mnl)}\cdot\mathbf{r}],\end{aligned} \tag{B1}$$

where L_x, L_y, and L_z are the dimensions of the hologram in x, y, and z directions, respectively, ϵ_{mnl} is the constant expressing the hologram strength of each component, and

$\mathbf{K}_g^{(mnl)}$ is the wave vector of the grating of each component. Therefore, along the same derivation path as that in Section 2, we can obtain the deformed dielectric modulation as

$$\Delta\epsilon(\mathbf{f}(\mathbf{r}')) \approx \Delta\epsilon(\mathbf{r}') + \sum_{m,n,l}\sum_{j=1}^{N} \frac{[\mathbf{K}_g^{(mnl)} \cdot A \cdot \nabla_{\mathbf{K}_g^{(mnl)}}]^j}{j!} \Delta\epsilon_{mnl}(\mathbf{r}'), \tag{B2}$$

where

$$\Delta\epsilon_{mnl}(\mathbf{r}') = \epsilon_{mnl} \exp(i\mathbf{K}_g^{(mnl)} \cdot \mathbf{r}'). \tag{B3}$$

The diffracted field after deformation will render the form

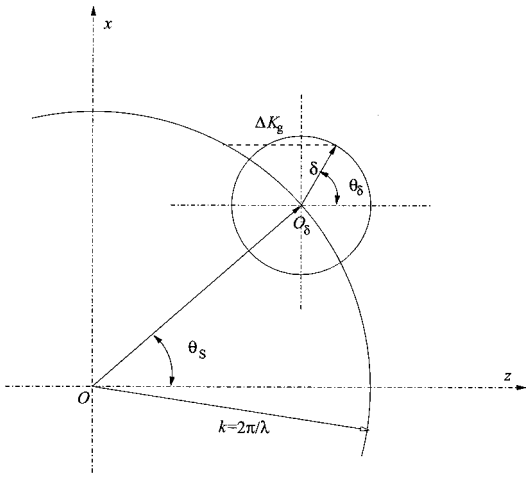

Fig. 14. Calculation of the locus of maximum Bragg mismatch.

$$\tilde{E}_d(\mathbf{r}'') \approx E_d(\mathbf{r}'') + \sum_{m,n,l} \int\int\int E_p(\mathbf{r}') \sum_{j=1}^{N} \frac{[\mathbf{K}_g^{(mnl)} \cdot A \cdot \nabla_{\mathbf{K}_g^{(mnl)}}]^j}{j!} \Delta\epsilon_{mnl}(\mathbf{r}') V(\mathbf{r}') \times \exp\left(-i\frac{2\pi}{\lambda}\frac{x'x'' + y'y''}{F}\right) \exp\left[-i\frac{2\pi}{\lambda}\left(1 - \frac{x''^2 + y''^2}{2F^2}\right)z'\right] d^3\mathbf{r}'. \tag{B4}$$

In the case of linear displacement, relation (B4) can be further simplified to

$$\tilde{E}_d(\mathbf{r}'') \approx E_d(\mathbf{r}'') + \sum_{m,n,l}\sum_{j=1}^{N} \frac{[\mathbf{K}_g^{(mnl)} \cdot A \cdot \nabla_{\mathbf{K}_g^{(mnl)}}]^j}{j!} E_d^{(mnl)}(\mathbf{r}''), \tag{B5}$$

where

$$E_d^{(mnl)}(\mathbf{r}'') = \int\int\int E_p(\mathbf{r}') \Delta\epsilon_{mnl}(\mathbf{r}') V(\mathbf{r}') \times \exp\left(-i\frac{2\pi}{\lambda}\frac{x'x'' + y'y''}{F}\right) \times \exp\left[-i\frac{2\pi}{\lambda}\left(1 - \frac{x''^2 + y''^2}{2F^2}\right)z'\right] d^3\mathbf{r}', \tag{B6}$$

$$E_d(\mathbf{r}'') = \sum_{m,n,l} E_d^{(mnl)}(\mathbf{r}''). \tag{B7}$$

Relations (B4) and (B5) are the counterparts of relations (16) and (17), respectively.

APPENDIX C: LOCUS OF MAXIMUM BRAGG MISMATCH

In this appendix we calculate the locus of maximum Bragg mismatch as a function of the deformation amount δ. As shown in Fig. 14, we want to find the point on the circle with center at O_δ and radius δ that has the maximum horizontal distance to the circle of the K-sphere. The horizontal distance represents the amount of Bragg mismatch $\Delta\mathbf{K}_g$. We can express the point on the circle of the K-sphere as

$$z^2 + x^2 = k^2, \tag{C1}$$

where $k = 2\pi/\lambda$, and the point on the circle O_δ as

$$(z - k\cos\theta_S)^2 + (x - k\sin\theta_S)^2 = \delta^2. \tag{C2}$$

The amount of Bragg mismatch is the horizontal distance between two points that have the same x coordinate and are on these two circles. This distance can be calculated as a function of x:

$$\Delta\mathbf{K}_g(x) = k\cos\theta_S + \sqrt{\delta^2 - (x - k\sin\theta_S)^2} - \sqrt{k^2 - x^2}. \tag{C3}$$

To get the maximum, we calculate the first-order derivative of Eq. (C3) and set it equal to zero:

$$\frac{\partial\Delta\mathbf{K}_g(x)}{\partial x} = -\frac{x - k\sin\theta_S}{\sqrt{\delta^2 - (x - k\sin\theta_S)^2}} + \frac{x}{\sqrt{k^2 - x^2}} = 0. \tag{C4}$$

Solving Eq. (C4), we obtain the x coordinate of the point, which has the maximum amount of Bragg mismatch, as

$$x_{max} = \frac{k^2\sin\theta_S}{k \mp \delta}, \tag{C5}$$

where $\pm$ means that there are two points that have the maximum amount of Bragg mismatch. One is in the interior of the K-sphere, the other is outside. Thus the maximum Bragg mismatch direction angle can be obtained as

$$\sin\theta_\delta = \frac{x_{\max} - k\sin\theta_S}{\delta} = \frac{\pm k\sin\theta_S}{k \mp \delta}. \quad \text{(C6)}$$

After knowing the maximum Bragg mismatch direction angle to different deformation amounts δ, we can sketch the locus of maximum Bragg mismatch as Fig. 4. When δ approaches zero, the maximum Bragg mismatch angle can be obtained as

$$\lim_{\delta\to 0} \sin\theta_\delta = \pm\sin\theta_S. \quad \text{(C7)}$$

This means that the fastest Bragg mismatch is obtained along the direction of the signal beam, which is consistent with the discussion in Section 2.

ACKNOWLEDGMENTS

We are grateful to Ondax, Inc. for providing holograms for the experiments, Wenyang Sun and Arnab Sinha for helpful discussions, and Jose A. Dominguez-Caballero for manufacturing the indenter tip holder. This project was funded by Defense Advanced Research Projects Agency/ Microsystems Technology Office.

The corresponding author's e-mail address is kehan@mit.edu.

REFERENCES

1. W. S. Colburn and K. A. Haines, "Volume hologram formation in photopolymer materials," Appl. Opt. **10**, 1636–1641 (1971).
2. B. L. Booth, "Photopolymer material for holography," Appl. Opt. **14**, 593–601 (1975).
3. D. H. R. Vilkomerson and D. Bostwick, "Some effects of emulsion shrinkage on a hologram's image space," Appl. Opt. **6**, 1270–1272 (1967).
4. P. Hariharan, *Optical Holography: Principles, Techniques, and Applications* (Cambridge U. Press, 1984).
5. N. Chen, "Aberrations of volume holographic grating," Opt. Lett. **10**, 472–474 (1985).
6. D. Gabor, "Microscopy by reconstructed wavefronts," Proc. R. Soc. London, Ser. A **197**, 454–487 (1949).
7. D. Gabor, "Microscopy by reconstructed wavefronts II," Proc. Phys. Soc. London, Sect. B **64**, 449–469 (1949).
8. X. Yi, P. Yeh, C. Gu, and S. Campbell, "Crosstalk in volume holographic memory," Proc. IEEE **87**, 1912–1930 (1999).
9. R. M. Shelby, D. A. Waldman, and R. T. Ingwall, "Distortions in pixel-matched holographic data storage due to lateral dimensional change of photopolymer storage media," Opt. Lett. **25**, 713–715 (2000).
10. D. Psaltis, D. Brady, G. Xiang-Guang, and S. Lin, "Holography in artificial neural networks," Nature **343**, 325–330 (1990).
11. C. Zhao, J. Liu, Z. Fu, and R. T. Chen, "Shrinkage-corrected volume holograms based on photopolymeric phase media for surface-normal optical interconnects," Appl. Phys. Lett. **71**, 1464–1466 (1997).
12. A. Sinha, W. Sun, T. Shi, and G. Barbastathis, "Volume holographic imaging in transmission geometry," Appl. Opt. **43**, 1533–1551 (2004).
13. E. N. Leith, A. Kozma, J. Upatnieks, J. Marks, and N. Massey, "Holographic data storage in three-dimensional media," Appl. Opt. **5**, 1303–1311 (1966).
14. A. A. Friesem and J. L. Walker, "Experimental investigations of some anomalies in photographic plates," Appl. Opt. **8**, 1504–1506 (1969).
15. P. Hariharan and C. M. Chidley, "Rehalogenating bleaches for photographic phase holograms: the influence of halide type and concentration on diffraction efficiency and scattering," Appl. Opt. **26**, 3895–3898 (1987).
16. P. Hariharan and C. M. Chidley, "Rehalogenating bleaches for photographic phase holograms: II. Spatial frequency effects," Appl. Opt. **27**, 3852–3854 (1988).
17. J. T. Gallo and C. M. Verber, "Model for the effects of material shrinkage on volume holograms," Appl. Opt. **33**, 6797–6804 (1994).
18. D. A. Waldman, H.-Y. S. Li, and M. G. Horner, "Volume shrinkage in slant fringe gratings of a cationic ring-opening holographic recording material," J. Imaging Sci. Technol. **41**, 497–514 (1997).
19. C. M. Vest, *Holographic Interferometry* (Wiley, 1979).
20. P. K. Rastogi, *Holographic Interferometry* (Springer-Verlag, 1994).
21. V. P. Shchepinov, V. S. Pisarev, S. A. Novikov, V. V. Balalov, I. N. Odintsev, and M. M. Bondarenko, *Strain and Stress Analysis by Holographic and Speckle Interferometry* (Wiley, 1996).
22. P. S. Theocaris, *Moire Fringes in Strain Analysis* (Pergamon, 1969).
23. A. J. Durelli and V. J. Parks, *Moire Analysis of Strain* (Prentice-Hall, 1970).
24. M. A. Kronrod, L. P. Yaroslavski, and N. S. Merzlyakov, "Computer synthesis of transparency holograms," Sov. Phys. Tech. Phys. **17**, 329–332 (1972).
25. U. Schnars and W. Juptner, "Direct recording of holograms by a CCD target and numerical reconstruction," Appl. Opt. **33**, 179–181 (1994).
26. Y. Pu and H. Meng, "An advanced off-axis holographic particle image velocimetry (HPIV) system," Exp. Fluids **29**, 184–197 (2000).
27. J. Zhang, B. Tao, and J. Katz, "Turbulent flow measurements in a square duct with hybrid holographic PIV," Exp. Fluids **23**, 373–389 (1997).
28. J. W. Goodman, *Introduction to Fourier Optics*, 2nd ed. (McGraw-Hill, 1996).
29. H. Coufal, D. Psaltis, and G. Sincerbox, eds., *Holographic Data Storage* (Springer, 2000).
30. C. Cohen-Tannoudji, B. Diu, and F. Laloë, *Quantum Mechanics* (Hermann/Wiley-Interscience, 1977).
31. K. L. Johnson, *Contact Mechanics* (Cambridge U. Press, 1985).